Astron. Astrophys. 355, 261–270 (2000)

ASTRONOMY AND ASTROPHYSICS

Spectropolarimetry of the symbiotic nova HM Sge⋆

H.M. Schmid[1,2], **R. Corradi**[3], **J. Krautter**[1], **and H. Schild**[4]

[1] Landessternwarte Heidelberg-Königstuhl, 69117 Heidelberg, Germany
[2] Max-Planck-Institut für Astronomie, Königstuhl, 69117 Heidelberg, Germany
[3] Instituto de Astrofisica de Canarias, c. Via Lactea S/N, 38200 La Laguna, Tenerife, Spain
[4] Institut für Astronomie, ETH Zentrum, 8092 Zürich, Switzerland

Received 14 October 1999 / Accepted 21 December 1999

Abstract. We present the first spectropolarimetric observations of the symbiotic nova HM Sge. We first note that marked spectral changes occurred: in the near IR the spectrum of the Mira in the system has clearly appeared. The nebular emission line spectrum remains largely unchanged but we detect for the first time the Raman line at λ6825. These changes indicate that the dust content in HM Sge is rapidly decreasing and that the dust obscuration period which began in 1985 has come to an end.

In terms of polarization we find that the red giant spectrum is intrinsically polarized at the 0.5 % level and the polarization signal is structured across the TiO absorption bands. The Raman scattered O VI line at λ6825 shows a polarization of 3.4 % at an angle of 33 °. The behaviour of the polarization angle across the Raman line strongly indicates that an axisymmetric O VI–H I scattering geometry prevails. The distribution of the neutral hydrogen in the inner binary system does not seem to be strongly perturbed by binary motion. We conclude that the present binary axis is orientated at a position angle of $\sim 123\,^\circ$.

The deduced orientation of the binary axis of HM Sge is parallel or perpendicular to distinct geometric features of the surrounding nebulosity. This indicates that the orientation of the binary system is of prime importance for the understanding of the nebular structure.

Key words: stars: binaries: symbiotic – stars: circumstellar matter – stars: mass-loss – polarization – scattering

1. Introduction

Dokuchaeva (1976) propelled an anonymous and faint light speck in the constellation of Sagitta into the select league of slow novae as she observed a sharp light increase and the appearance of emission lines on an objective prism plate taken with the Schmidt camera of the Piszkesteto Observatory in Hungary. The spectral evolution of the object, since then known under the name of HM Sge, was followed in much detail. In the first decade after the outburst observations revealed a steady increase in the ionization degree of the emission nebula in step with the evolution of the temperature of the hot component (e.g. Stauffer 1984; Nussbaumer & Vogel 1990; Mürset & Nussbaumer 1994 and references therein). Since about 1987 this evolution came to a halt and the emission line spectrum remained practically unchanged.

HM Sge is a dust rich or D-type symbiotic system that contains a Mira variable. The Mira period, as measured from JHK photometry, is 527 days. Beyond the Mira variability, Munari & Whitelock (1989) detected in the JHK bands a gradual fading which they attributed to a dust obscuration event. The decrease in IR brightness started in 1985 and continued until at least 1993 (Yudin et al. 1994). Recent IR observations indicate that the trend has reversed now (Kamath & Ashok 1999). Similar dust obscuration episodes have occurred in other symbiotics but not in single Miras. Their cause is probably related to the binarity of symbiotic stars. It was suggested that different viewing angles due to binary rotation may produce the effect but other causes could also be responsible. Possibly the dust distribution is more patchy in the circumstellar environment of symbiotic Miras or colliding winds generate a compression wave which can efficiently produce large amounts of dust.

The extinction towards the Mira is much larger than that of the nebular emission region. This can be taken as indication that the hot and ionizing component is not obscured by the dust shell of the cool component. Also the dust does not appear to survive in the ionized region since the abundances of dust forming elements are not depleted (Schmid & Schild 1990).

Extended nebular emission associated with HM Sge was detected in optical images, UV-images with HST, and with radio interferometry. Radio interferometry revealed the evolution of a compact, central nebulosity from about 0.15″ in 1982 (Kwok et al. 1984) to two parallel ridges about 0.1″ north and south of a deep central minimum in 1992 (Eyres et al. 1995). The 1992 radio map shows a good correlation with (practically) simultaneous HST UV images apart from the central minimum, which is a strong maximum in the UV filter F190M (Hack & Paresce 1993). Further radio maps described in Richards et al. (1999) indicate that the emission features are not just expanding but seem to rotate in an anti-clockwise direction. The radio struc-

Send offprint requests to: H.M. Schmid (hschmid@lsw.uni-heidelberg.de)

⋆ Based on observations taken with the 4.2m William Herschel Telescope at La Palma and the 2.3m ANU Telescope at Siding Spring.

ture of the nebulosity seems to be very complex and a simple interpretation in terms of e.g. colliding wind models seems difficult. The central features are surrounded by a complex, weak structure which is elongated east-west and extends to about $1''$ from the central source. This region includes two spots with non-thermal emission about $0.6''$ east and west of the central source (Eyres et al. 1995; Richards et al. 1999). On the same scale a bipolar outflow in the [N II] lines was detected by Solf (1984) with radial velocities of ± 46 km/s at a position angle of about $-60°$. In very deep [N II] and [O II] images additional structures at larger distances are seen, including even a jet-like structure extending to about $10''$ from the center (Corradi et al. 1999). All these maps provide a unique view on the flow patterns that emerged from the nova outburst and which, in the future, will further modulate the circumstellar environment and ultimately lead to a large scale nebula. The structures and the evolution of such symbiotic systems attracts currently much attention as they are thought to be good candidates for the progenitors of bipolar planetary nebulae (e.g. Corradi & Schwarz 1995, 1997).

In this paper we report about recent changes in the optical and NIR spectrum of HM Sge and present the first spectropolarimetric observations. We note that the red giant has re–emerged and find that the dust column in the line of sight has markedly decreased. Our data reveal also the polarization in the Raman scattered O VI lines which were not seen before in this object. After describing our observations in Sect. 2 we discuss the spectral changes in detail. Sects. 4 and 5 deal with the spectropolarimetric results. First we discuss issues of the continuum polarisation, including the interstellar polarisation and then turn to the Raman line polarisation. Our results are finally summarised in the last section.

2. Observations

WHT observations, June 1998. We observed HM Sge spectropolarimetrically during the two nights of June 29 to July 1, 1998 with the 4.2m William Herschel Telescope (WHT) on La Palma, Canary Islands. During the first night the red arm of the ISIS spectrograph/polarimeter was used with the R158R grating, which provided coverage from about 6400 to 9400 Å with a resolution of ~ 6.5 Å. These observations revealed the presence of the Raman scattered O VI lines and an unexpectedly strong continuum of the red giant. Therefore we subsequently used the ISIS blue arm with the R300B grating yielding a resolution of $\sim$ 3.5 Å in the range from 3300 to 6300 Å. Additional polarimetric data of the Hα and Raman line region were obtained with the ISIS red arm and grating R600R providing a spectral coverage from 6450 to 7250 Å with a resolution of 1.6 Å. The spectral resolutions were derived from the width of narrow emission lines (FWHM) in HM Sge and other targets. They are in good agreement with the measured size of the seeing disk of about $0.8'' - 1.0''$ For the red spectra a 1124×1124 TEK CCD was used and the blue spectra were recorded with a 2148×4200 EEV CCD.

For all observations a rotatable half-wave plate and a calcite block were inserted into the beam to measure the linear polarization. One measurement consists of a set of four observations taken at half-wave plate angles of $0°$, $45°$, $22.5°$ and $67.5°$. The calcite block generates two beams with perpendicular polarization. Exposures with the half-wave plate at $0°$ and $45°$ yield Stokes Q and the other two yield Stokes U.

In the continuum of HM Sge we detected typically $10^4 - 2 \cdot 10^4$ counts and the S/N was therefore dominated by photon noise. As a consequence of the high exposure level, some emission lines were saturated. With the R158R grating we have taken two cycles of observations, one with 90 s exposure time at each half-wave plate position and one with 15 s. Even in the shorter exposures the Hα line was saturated, and six further lines were overexposed in the 90 sec cycle. The 4×150 s cycle taken with the R600R grating saturated Hα, [N II]λ6584 and [Ar III] λ7136. Twelve lines are saturated in the 4×600 s ISIS blue arm data.

The observations were reduced by standard techniques with the MIDAS software available at the Landessternwarte in Heidelberg. We paid particular attention to a careful subtraction of the scattered light halos around very strong emission lines (Hα and Hβ/[O III]-region), which contaminated the adjacent spectral regions and also the accompanying parallel spectrum with the perpendicular polarization. In principle, no flatfielding information is needed with this type of polarization measuring technique. However, strong interference fringes are present in the R158R grating data above 8000 Å and we found that flatfielding improved the quality of these data. The eight spectra from a given cycle were then combined in a standard way to yield the relative Stokes parameter spectra Q/I and U/I (see Schmid & Schild 1994; Tinbergen & Rutten 1997). As we are not interested in absolute intensity information no flux calibration was applied.

The polarized standard stars HD 154445, HD 204827 (Hsu & Breger 1982) and the unpolarized standards HD 154892, BD+32°3739 (Turnshek et al. 1990) were used to check and correct for the intrumental polarization. The instrumental calibration is estimated to be accurate to $\theta \approx 1°$ for the angle and to $p \approx 0.1\%$ for the percentage polarization.

Previous observations. We compare these observations with earlier data of HM Sge that we obtained with the WHT and the ANU 2.3m telescope of the Siding Spring Observatory (SSO).

WHT spectropolarimetry was gathered during the nights of July 21, 1993 and July 15, 1995 with the ISIS red arm. Observational details can be found in Schmid & Schild (1997).

At the ANU 2.3m Telescope of the Siding Spring Observatory (SSO) we collected spectroscopic observations in April 1994 with the Double Beam Spectrograph (DBS). For the red arm of the DBS we used a grating with 158 lines/mm providing a spectral coverage from 6300 – 10300 Å and a resolution of 4 Å/pixel or a FWHM of ≈ 8 Å for the lines of a HeAr calibration lamp. The blue arm of the DBS recorded simultaneously a spectrum from 3300 Å to 5300 Å with a resolution of about 6 Å (FWHM) using a grating with 300 lines/mm.

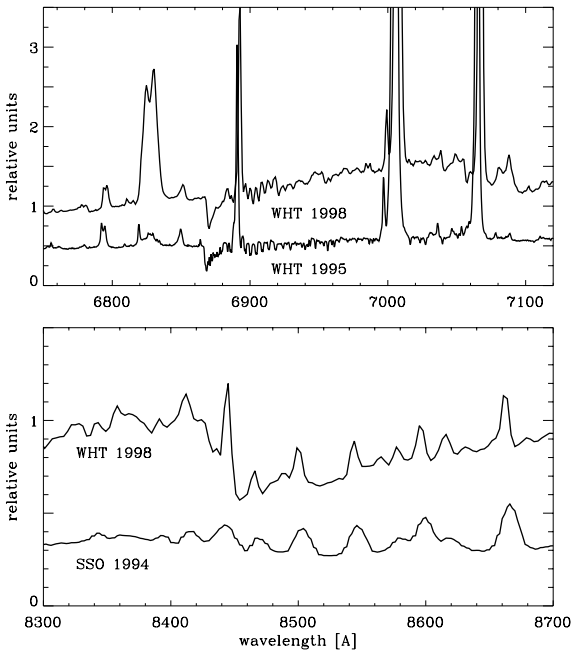

Fig. 1. Changes in the spectrum of HM Sge. Top panel: appearance of the Raman scattered emission line at λ6825 between July 1995 and June 1998. Lower panel: Strengthening of the TiO absorption band at λ8432 and of the O I λ8446 fluorescence line emission (e.g. relative to the H I Paschen lines) between April 1994 and June 1998.

3. Spectroscopic evidence for decreasing dust absorption

3.1. Spectral features of HM Sge

Our present observations of HM Sge cover the spectral range from about 3300 to 9400 Å. In this region the spectrum shows strong lines from an emission nebula, a practically featureless nebular continuum below 6000 Å and a red giant spectrum which dominates the continuum emission above 8000 Å. Towards shorter wavelengths the emission of the red giant decreases strongly but the TiO band at 6150 Å is still detectable. We estimate that the red giant contributes at this wavelength $\sim$10% to the total continuum. Thus, further to the blue, the continuum is close to 100% due to the emission nebula.

The emission line spectrum of HM Sge shows very strong [O III] and Balmer lines. Further prominent features are lines from He I, He II, [N II], [O I], [Ne III], [S III], [Ar III], [Ar V] and [Fe VII] and numerous weaker emission lines. A detailed description of the emission line spectrum of HM Sge can be found in Schmid & Schild (1990).

3.2. The rise of fluorescent O I and Raman scattered O VI line emission

Our present observations and the SSO spectra taken in April 1994 reveal that the nebular emission line intensities remained largely unchanged. We only detect small variations below the 20 %-level, for almost all emission lines. This includes more than 30 unsaturated prominent lines between 3800 to 5200 Å and 6400 to 9400 Å. The nebular emission dominates strongly the intensity of HM Sge in the UBVR-region. As the corresponding light curves stayed practically constant since more than a decade, we can conclude from the constant relative line fluxes that also the absolute line fluxes remained largely unchanged. However, three lines display an outstanding flux increase between April 1994 and June 1998, namely O I λ8446 and the two Raman scattered O VI lines at $\lambda\lambda$6825,7082 (Fig. 1). A further feature that showed a 50 % increase is the line at 4247.4 Å, for which we found no convincing identification (the wavelength of a transition of C III (11) would match, however it's not clear how this two-electron transition could reach the line strength observed in HM Sge).

The O VI Raman lines at λ6825 and λ7082 are to our knowledge new features in the HM Sge spectrum. We have already spectropolarimetrically searched for these lines with the WHT in 1993 and 1995 but we found, besides a small, narrow emission line near λ6819, only a very weak and unpolarized feature. The same emission was already noted by Stauffer (1984) and interpreted as broad λ6825 emission, which was at that time unidentified. However, these weak features were probably not due to Raman scattered O VI emission because, firstly they were not polarized ($p < 0.2\%$ in 1993 and 1995), and secondly there were narrow spectral sub-features. This is hardly compatible with the O VI Raman scattering process (Schmid 1989) and we conclude that the Raman scattered lines newly appeared between July 1995 and June 1998.

In April 1994 the H I Paschen Series was barely disturbed by the O I emission (Fig. 1, bottom panel). The P18 line at 8438 Å is slightly too strong compared to the adjacent members P17 8467.3 Å and P19 8413.3 Å due to the presence of a weak O I contribution. Contrary to this the O I/P18 line blend is much stronger than the other Paschen lines in the June 1998 spectrum. The O I λ8446 line has increased from April 1994 to June 1998 by a factor of about $5 - 10$ relative to the H I Paschen lines. In the June 1998 spectrum the flux of the O I/P18 blend is $F(\mathrm{OI/P18}) = 2.9 \cdot F(\mathrm{P15}\,\lambda 8545)$. It is interesting to note that the O I λ8446 line was shortly after the outburst until about 1981 much stronger than the neighboring Paschen lines (see Stover & Sivertsen 1977; Ciatti et al. 1977; Andrillat 1982). The O I line faded thereafter, probably in connection with the dust obscuration phase which started around 1985 (Munari & Whitelock 1989).

The strength of the O I λ8446 and the Raman scattered O VI lines depends on the flux of far-UV line emission in the neutral region. O I is the result of a line fluorescence effect where H I Lyβ λ1025.72 photons excite O I via a resonance transition at λ1025.76 to a highly excited level. The subsequent cascade route leads to O I emission lines at λ11287, λ8446 and λ1304 (Bowen 1947; for more details see e.g. Grandi 1980; Kastner & Bhatia 1995). The O VI Raman features are the product of the excitation of neutral hydrogen to an intermediate virtual state near the $3p$-state by far-UV O VI $\lambda\lambda$1032,1038 photons, from where hydrogen decays to the $2s$-state by emitting the lines at λ6825 and λ7082 (Schmid 1989).

The sudden increase of these lines can be explained by a strong decrease of the dust absorption of the far-UV emission

lines Lyβ and O VI in or near the neutral region. Dust absorption is very efficient and changes in the dust density can cause order of magnitude changes in the UV-flux level in the neutral region. Other processes could in principle also produce a flux change in the O I and Raman scattered O VI lines, but the fact that both types of lines react simultaneously excludes other simple explanations. For example an ionization effect can hardly produce the same behavior for features with so strongly different ionization potentials as O I and O VI. Also, specific changes in gas velocities could modify the efficiency of the radiative transfer in the O I line fluorescence, but not in the O VI Raman scattering which behaves like a continuum process.

Furthermore, a drastically reduced dust absorption for the far-UV emission lines Lyβ and O VI as explanation for the marked increase of the O I fluorescence and O VI Raman lines is also strongly supported by the simultaneous (re)-appearance of the red giant emission in the red spectral region (see below).

3.3. The appearance of the Mira spectrum

We find that the red giant spectrum has brightened enormously in HM Sge and that the red giant absorption features are much more conspicuous than in earlier observations (Fig. 1). In Fig. 3 we compare a section of our June 1998 spectrum with the spectrum from April 1994. The spectra have been scaled such that the emission line fluxes agree best. The strong increase of the red giant spectrum is clearly evident. We found in the literature no other observations of HM Sge taken since 1985 where the 7500 to 9500 Å range shows similarly strong red giant features as in our June 1998 observations. From about 1985 to about 1996 strong absorption features from the red giant were only visible in the $1\,\mu$ region (Rudy et al. 1999; Mürset & Schmid 1999). Beyond $2\,\mu$ the emission of dust dominates the near IR-spectrum (Schild et al. 1992). Before 1984 the red giant absorptions features e.g. TiO 8430 Å, were stronger than between 1985 and 1998 as can be seen from the spectrum of Schulte-Ladbeck (1988) taken in July 1983. Below we will provide evidence that the time interval 1985 – 1998 with a weak red giant continuum coincides with a dust obscuration phase of the Mira in HM Sge.

Of course, brightness changes can also be expected due to the Mira variability of the red giant in HM Sge, which has a period of about 527 days. However, according to the pulsation ephemeris of Yudin et al. (1994) the phases of the observations of June 1998 ($\phi = 0.85$) and April 1994 ($\phi = 0.96$) are almost the same and close to the minimum phase ($\phi = 0$). Even the WHT-spectrum from July 1995 which was taken at maximum of the pulsation phase ($\phi = 0.5$) shows no signs of the λ7054 TiO bands, while it is clearly visible in the June 1998 data (see Fig. 1).

IR-photometric observations also point to a reduced dust extinction as cause for the sudden brightening of the red giant in HM Sge. The IR light curves, especially for the J-filter, show beside the periodic Mira variations also a fading event starting in 1985 and lasting to at least 1993 (Munari & Whitelock 1989; Yudin et al. 1994). New IR-measurements taken in May 1997 near minimum phase ($\phi = 0.07$) by Kamath & Ashok (1999) indicate a J-band brightness increase to J = 7.36, which is about 1.4 mag brighter than the minimum magnitudes measured during the previous IR faint phase. A brightness increase of 1.4 mag in the J-band due to a reduction in dust absorption would translate to a brightness increase of about 3 mag in the R-band adopting the standard (i.e. interstellar) dust extinction law. As can be seen in Fig. 3 such a flux increase by at least a factor of 10 has indeed taken place in HM Sge.

4. Continuum polarization

4.1. Spectropolarimetric components

The relative Stokes spectra Q/I and U/I of HM Sge show three main polarization components (Fig. 2):

- For wavelengths < 6000 Å the polarization is practically constant at $Q/I \approx 0.1\%$ and $U/I \approx 1.1\%$. The U/I-spectrum shows a slow decrease but remains featureless up to 9400 Å apart from the strong peak at 6825 Å. Such a smooth shape is typical for an interstellar polarization component.
- Above 8000 Å there are strong polarimetric signatures of about -0.5% in the Q/I-spectrum which reflect the highly structured absorption features of the cool giant in the intensity spectrum (Fig. 2). This polarization signal must be intrinsic to HM Sge and seems to be caused by scatterings of the light from the cool giant.
- The third feature is the outstanding polarization signal due to the Raman scattered line O VI λ6825, which in the intensity spectrum is just a rather inconspicuous emission line. The polarization signal of this line reflects the O VI Raman scattering geometry in the HM Sge system.

Before we further discuss these polarization components we give some technical details about how the polarization spectrum in Fig. 2 was obtained.

In order to enhance the S/N-ratio of the relative Stokes-spectra we have binned our low resolution data (R300B and R158R) with a bin size of 50 Å. The red portion of the polarization spectrum is based on the cycle with 90 s exposure time, except for the intervals containing a saturated line, where we inserted the 15 s data points. The polarimetric signal in the R600R observations is consistent with the R158R data. We excluded Hα, for which we have no unsaturated observation as well as all bins containing saturated lines in the ISIS blue arm data.

The achieved accuracy in Q/I and U/I in a given spectral bin depends on the count rate, which can vary strongly. For $\lambda > 8000$Å there is in addition a small uncertainty due to a very weak remaining pattern from the interference fringes. The residuals (1σ) of the U/I-spectrum relative to a smooth line indicate that an accuracy of typically 0.1% per bin is achieved (Fig. 2).

The possibility that the emission lines have a different polarization than the continuum has been carefully considered. We found no significant difference $> 0.2\%$ in polarization between

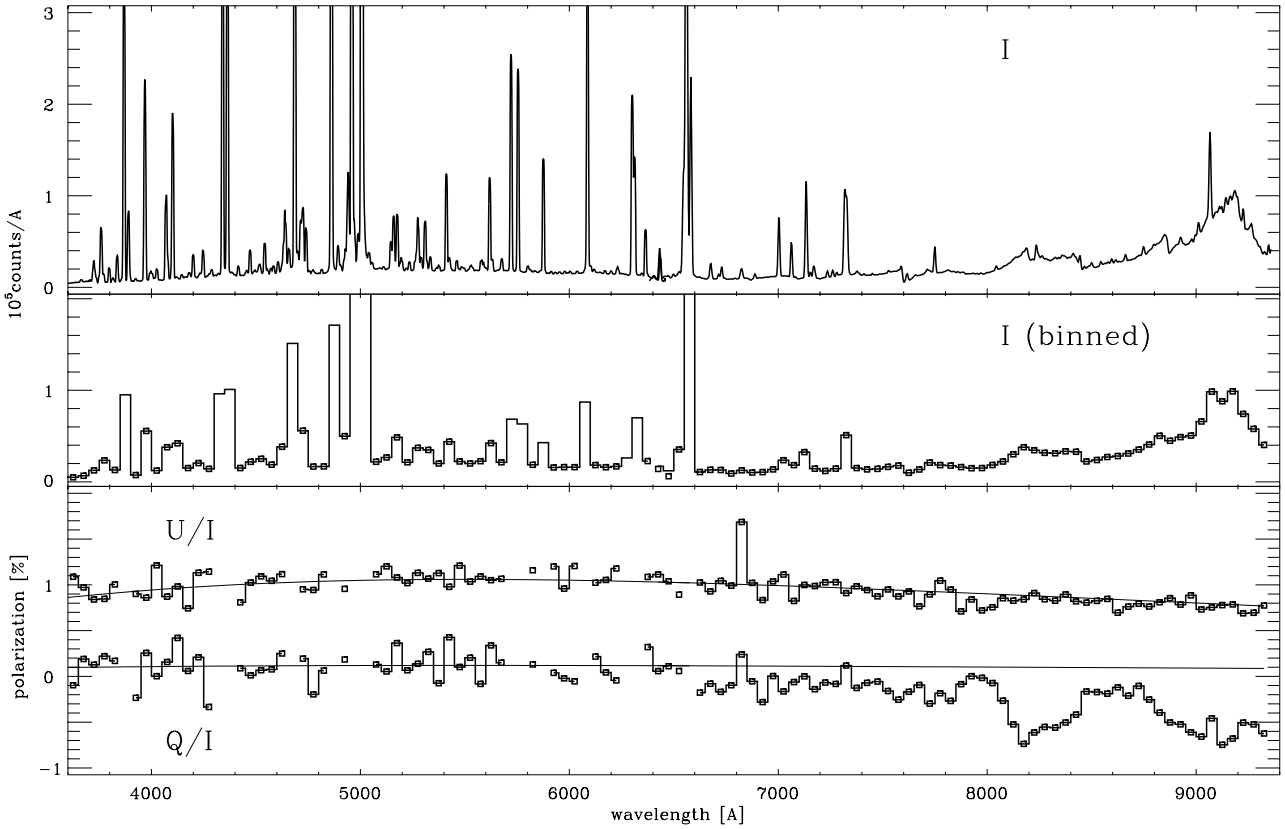

Fig. 2. Low resolution spectropolarimetry of HM Sge. From top to bottom: observed intensity (count spectrum), binned intensity, relative Stokes spectra Q/I and U/I. The smooth lines in the bottom panel give the adopted interstellar polarization component. Strong intrinsic polarization is seen at λ6825 for the Raman scattered O VI line and at $\lambda > 8000$ Å in the Q/I spectrum from the red giant.

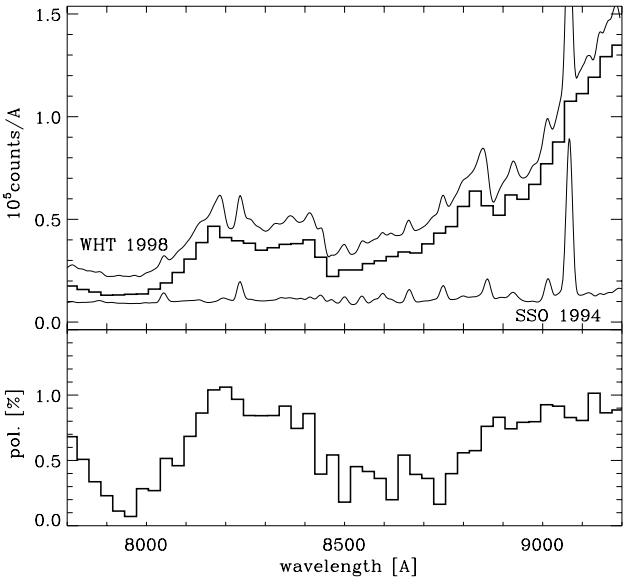

Fig. 3. Intrinsic polarization for the Mira variable in HM Sge. The upper panel compares the red spectrum of HM Sge from June 1998 with strong molecular absorption features with the almost pure nebular emission observed in April 1994. The thick curve gives the binned red giant spectrum (30 Å bins) obtained by subtracting the latter from the first spectrum. The lower panel shows the resulting (photospheric) polarization structure of the Mira variable.

spectral intervals containing strong, unsaturated lines and intervals with only weak line emission. The only exception is the O VI Raman line λ6825 which will be discussed below. Further we see a depolarization of the intrinsic continuum polarization of the red giant in the Q/I-spectrum at the position of the strong [O II] λ7325 and [S III] λ9069 emission lines. This indicates that these emissions are intrinsically unpolarized as expected for nebular lines (assuming negligible scattering in a circumnebular region). Thus, it seems safe to assume that the nebular lines represent just the interstellar polarization component.

4.2. Comparison with broad-band polarimetry

In order to facilitate a comparison with earlier filter polarimetry we give mean polarization values from our unsaturated bins for the wavelength intervals (in μm) [0.4,0.5], [0.5,0.6], [0.6,0.75] and [0.75,0.93] which correspond very roughly to the B, V, R and I filters. The results are listed in Table 1, together with literature values from Efimov (1979), Schulte-Ladbeck (1985) and Johnson & Jones (1991). Efimov (1979) gave polarimetry for 6 observing dates in 1977 and 1978 which all showed a similar polarization pattern. We only use the mean values which are sufficient for our long term comparison. It should, however, be noted that there are also short term variations in the Efimov-data, especially in the U band, which point to intrinsic vari-

Table 1. HM Sge polarization in broad band filter regions from the literature and our WHT spectropolarimetry. For the Efimov (1979) observations only the mean of 6 runs is given. The last columns give the adopted interstellar polarization at about the central wavelength of the corresponding broad band filters.

Efimov mean 1977/1978		Schulte-Ladbeck date: Sep/Oct 1983		Johnson & Jones date: Aug/Oct 1988		WHT (this work) date: June 1998		interstellar pol. (adopted)	
filter	p[%] / $\theta[^\circ]$	filter	p[%] / $\theta[^\circ]$	filter	p[%] / $\theta[^\circ]$	interval	p[%] / $\theta[^\circ]$	λ	p[%] / $\theta[^\circ]$
U	0.89 / 32	U	0.88 / 52	U	0.96 / 48			3500	0.84 / 42
B	0.89 / 38	B	1.05 / 53	B	1.09 / 48	[4000:5000]	1.01 / 43	4500	1.01 / 42
		[OIII][a]	1.03 / 44						
V	1.01 / 41	V	1.08 / 47	V	1.12 / 51	[5000:6000]	1.10 / 41	5500	1.06 / 42
		λ6360[a]	1.54 / 48						
		Hα[a]	1.21 / 52						
R	1.13 / 49			r	1.12 / 46	[6000:7500]	1.05 / 46	6750	1.01 / 42
		λ7980[a]	1.07 / 62						
		I	0.49 / 65	i	0.99 / 43	[7500:9300]	0.89 / 56	8400	0.86 / 42
				J	0.75 / 61			1.25μ	0.49 / 42
				H	1.14 / 72			1.62μ	0.28 / 42
				K	1.18 / 76			2.20μ	0.08 / 42
err.[b]	$\sim$0.15 / $\sim$5	err.[b]	$\sim$0.07 / $\sim$3	err.[b].	$\sim$0.12 / $\sim$3	err.	$\sim$0.10 / $\sim$3		

a: polarization in narrow band filters; b: typical errors in broad band filters – for details see the original papers.

ability. There is good agreement ($\Delta p \lesssim 0.1\,\%$, $\Delta\theta \lesssim 10^\circ$) in the V- and R-filter region between the different observations given in Table 1. Although not very sensitive the WHT observations taken in 1993 and 1995 indicate an upper limit of $\Delta p \lesssim 0.5\,\%$ for polarimetric variations in the continuum around 7000 Å for more recent years.

Contrary to this the U and B measurements indicate significant polarization variability, particularly between 1977/1978 and 1983. These changes could be related to the 1975 outburst of the hot component in HM Sge. Also in the I-band region the data indicate strong long term variability. This is not surprising as this region includes the intrinsic polarization component of the Mira variable. Even if the relative intrinsic polarization of the Mira is constant in time the measured polarization would vary due to the changing contribution of the Mira emission to the total light.

In spite of these variations, all data sets indicate a similar polarization angle rotation toward NIR/IR wavelengths which is due to the predominant position angle of roughly $\sim 90^\circ$ for the intrinsic polarization of the cool component (see below).

4.3. Interstellar polarization

The interstellar polarization is expected to be constant in time and to show a smooth, characteristic wavelength dependence of the percentage polarization $p_{\rm is}$ at a constant position angle $\theta_{\rm is}$. The wavelength dependence of $p_{\rm is}$ can be described by the well known Serkowski law (Serkowski et al. 1975)

$$p_{\rm is}(\lambda) = p_{\rm max} \exp\{-1.15\,[\ln(\lambda_{\rm max}/\lambda)]^2\}\,,$$

$p_{\rm max}$ is the maximum polarization at the wavelength $\lambda_{\rm max}$ which typically occurs at 5500 Å.

In our spectropolarimetric observations of HM Sge the wavelength region below 6000 Å shows such a smooth wavelength dependence, no rotation in the polarization angle and only very little temporal variability. We thus attribute this polarization component to the interstellar medium. By chance, the position angle $\theta_{\rm is}$ is close to $\sim 45^\circ$ which is the Stokes $+U$ direction. The intrinsic polarization component of the cool giant is seen in the Stokes $-Q$ direction or at a position angle of $\theta \approx 90^\circ$, while no similar signatures occur in the Stokes U/I-spectrum. In fact, the U/I-spectrum is consistent with pure interstellar polarization even at longer wavelength.

Fitting Serkowski-curves with $\lambda_{\rm max} = 5500$ Å to the U/I-spectrum gives $(U/I)_{\rm max} = +1.06\%$ as best fit result with a 1σ-residual of about 0.1% (see Fig. 2). Changing the value of $\lambda_{\rm max} = 5500$ Å gives no significant improvements. The Q/I-spectrum below 6000 Å shows a small, constant component at the $\sim +0.1\%$-level. The polarization signal in Q/I is too low to identify a spectral dependence. However, we see also no features which might indicate a polarization component intrinsic to HM Sge. Fitting Serkowski-curves to this spectral range gives $(Q/I)_{\rm max} = +0.12\%$ as best result (Fig. 2). Expressed as percentage polarization and position angle we obtain for the interstellar polarization component $p_{\rm max} = 1.06 \pm 0.05\%$ and $\theta_{\rm is} = 42 \pm 3^\circ$. This assumes that there is no intrinsic polarization component in the spectral region from 3800 to 6000 Å.

This result is largely supported by previous polarimetric work of Schulte-Ladbeck (1985) and Johnson & Jones (1991). They measured the same percentage polarization in the UBV filters and a position angle close to our value. However, the small difference of about 8° in $\theta_{\rm is}$ is significant. This may point to a small and variable $p \approx 0.2\%$ polarization component intrinsic to HM Sge, which could be present in either the earlier polarimetric observations, in our observations or even in both.

We believe that the polarization below 6000 Å in our 1998 observations represents best the pure interstellar component. This follows mainly from the absence of any signs for an in-

trinsic polarization component in our data. Between 1977 and 1983, rather strong polarimetric variations $\Delta p > 0.2\%$ and large position angle rotations of about $45°$ and $30°$ in the V and U-bands were observed. At that time, just a few years after outburst, the hot component was rather strong in the UV (see Nussbaumer & Vogel 1990) and could well have contributed to a polarization signal. The polarimetric measurements taken by Schulte-Ladbeck (1985) might still be affected particularly in the U and B-region. This interpretation is supported by the polarization measurement in the [O III] filter of Schulte-Ladbeck (1985), which can be interpreted as depolarization effect of a small intrinsic signal by strong (intrinsically unpolarized) nebular emission.

Based on these considerations we adopt for the interstellar polarization the Serkowski-curve fit to our spectropolarimetric data with the parameters given above. Values of $p_{\rm is}(\lambda)$ are listed in Table 1.

4.4. Intrinsic polarization of the the red giant

The red giant produces a negative polarization signal in the Stokes Q/I-spectrum (see Fig. 2). The U/I-spectrum, on the other hand, does not show any deviation from the smooth interstellar polarization law. This indicates that the position angle of the intrinsic polarization component of the red giant coincides to within $5°$ with $\theta = 90°$ Therefore, the U/I-component is practically zero and can be neglected, so that the intrinsic percentage polarization of the red giant is $p_{\rm rg} = |(Q/I)_{\rm rg}|$.

First, we have to correct the Stokes Q/I-component $(Q/I)_{\rm cor} = (Q/I) - (Q/I)_{\rm is}$ for the interstellar polarization $(Q/I)_{\rm is}$ which is plotted in Fig. 2. Then the nebular contribution to the intensity spectrum is subtracted, so that we get the emission of the red giant $I_{\rm rg} = I - I_{\rm neb}$. The emission lines are easy to remove, and to correct for the continuum, we subtract the continuum of our April 1994 spectrum which is purely nebular (see Fig. 3). The intrinsic polarization for the red giant is then obtained according to $(Q/I)_{\rm rg} = Q_{\rm cor}/I_{\rm rg}$, where $Q_{\rm cor} = I \cdot (Q/I)_{\rm cor}$, is the Stokes Q-component corrected for the interstellar polarization. We thus assume that the nebular emission is intrinsically unpolarized.

The resulting intrinsic polarization for the red giant is plotted as binned polarization spectrum $p_{\rm rg} = |(Q/I)_{\rm rg}|$ in the lower panel of Fig. 3. Clearly $p_{\rm rg}$ varies with wavelength. We have $p_{\rm rg} \approx 0.9\%$ in the range $8100 - 8400$ Å and $8900 - 9400$ Å, but only $p_{\rm rg} \approx 0.4\%$ for the region $8500 - 8800$ Å which coincides with a strong TiO absorption band. From possible error sources in our applied procedures we estimate that the polarization spectrum $p_{\rm rg}$ could be affected by a systematic error of about 0.1% or/and a factor of about 1.2. However, the spectral signature of the red giants' intrinsic polarization is practically independent of these uncertainties. At shorter wavelengths of $7000 - 8000$ Å the low intensity of the red giant makes $p_{\rm rg}$ difficult to determine. However, the signal is still consistent with $p_{\rm rg} \approx 0.2 - 1.0$ as for $\lambda > 8000$ Å.

The fact that the polarization $p_{\rm rg}$ in the strong TiO band around 8500 Å drops to about half the value of the adjacent continuum indicates, that the polarization is predominantly due to photospheric inhomogeneities of the Mira variable. A similar dependence between molecular absorption and polarization signal is known to be often present in Mira variables (e.g. Landstreet & Angel 1977; Coyne & Magalhaes 1979; Boyle et al. 1986; Trammell et al. 1994).

Polarization due to light scattering in a circumstellar dust shell is expected to produce a smooth spectral signal. Such a circumstellar polarization component can only be hidden in our spectropolarimetric data, if the percentage polarization is either small $< 0.2\%$ or if the polarization angles of the circumstellar and the photospheric components coincide. As the latter case seems to be unlikely we conclude that, in terms of polarization, circumstellar scatterings are not important.

5. The polarization in the Raman line

Although the Raman scattered O VI line at λ6825 is relatively weak in intensity, it produces an outstanding signal in the polarization spectrum. Fig. 4 shows the observed (unbinned) spectropolarimetric structure. The intensity profile is double–peaked and has a FWHM of ≈ 15 Å (see also Fig. 1).

5.1. Line profile extraction

In order to extract the intrinsic polarization of the Raman lines at λ6825 and λ7082 a similar procedure is applied as for the intrinsic polarization of the red giant. To correct for the interstellar polarization, we use the flux weighted mean of the relative Stokes parameters Q/I and U/I, measured in the interval $6850 - 7050$ Å. This accounts correctly for the interstellar polarization if the underlying continuum is intrinsically unpolarized. Also an offset in the Q/I and U/I calibration, which is however expected to be less than 0.2%, would be compensated. The low resolution data indicate that there could be an intrinsic continuum polarization component from the red giant of at most -0.2% in Q/I. If real this would introduce a small error of $\approx 0.1\%$ in the resulting Q/I polarization of the Raman lines. This uncertainty is small and uncritical, when compared to the strong polarization of more than 3% in the λ6825 Raman line. Even the uncertainties in the weakly polarized red wing of the λ6825 line are still dominated by photon noise.

The Raman line intensity profiles are obtained by a subtraction of the expected continuum. The TiO triple band head at λ7052, which is veiled by the nebular continuum but still visible, has also been removed from the λ7082 profile.

5.2. Intrinsic polarization structure

The integrated (flux weighted) intrinsic polarization of the λ6825 line is $p = 3.6 \pm 0.4\%$, $\theta = 33° \pm 3°$ for the low resolution, and $p = 3.1 \pm 0.4\%$, $\theta = 34° \pm 3°$ for the medium resolution data. In the following we adopt $p = 3.4\%$, $\theta = 33°$, giving slightly more weight to the low resolution data. The polarized flux in the λ7082 line is too weak to be measured accurately.

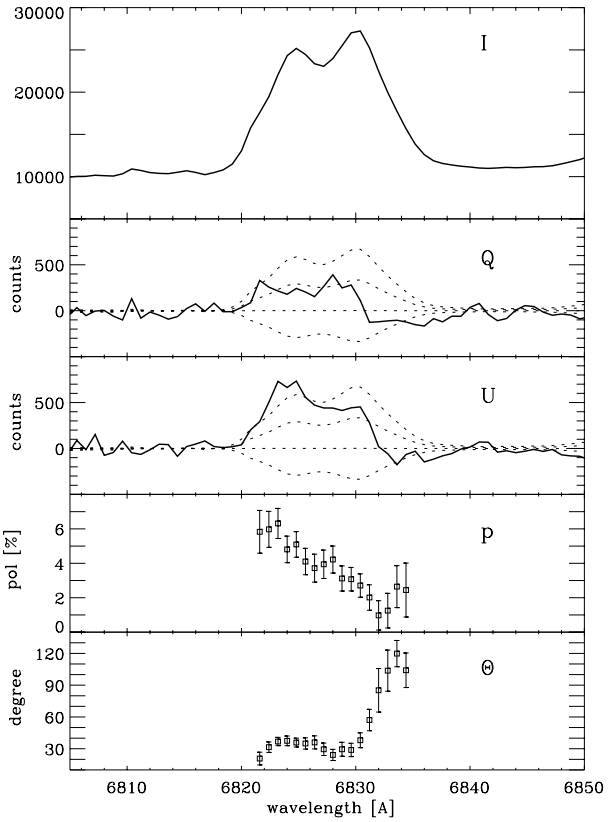

Fig. 4. Spectropolarimetric structure of the Raman line λ6825 in HM Sge. The top panel gives the intensity spectrum. The second and third panel show the intrinsic Stokes Q and U profile, together with continuum subtracted Raman line intensity curves with scaling parameters -0.02, 0.0, 0.02 and 0.04 (dotted lines). The two bottom panels give the intrinsic percentage polarization p and the position angle θ for the Raman line. The error bars account only for the photon noise, which are much larger than possible systematic errors.

The very noisy signal leads to $p \approx 3 \pm 2\%$ and $\theta = 30° \pm 30°$ which is compatible with the polarization in the λ6825 line.

The polarization structure of the stronger Raman line is shown in Fig. 4 as Stokes parameter Q and U and as percentage polarization p and position angle θ. The photon noise level is well visible in the Q and U data. The error bars for p and θ account for this photon noise. They are particularly large in the weak line wings and in the case of θ also for points with low p-values. We recall that the systematic errors are estimated to be $\lesssim 0.2\%$ in p, Q/I and U/I.

The λ7082 feature is too weak for a meaningful analysis of its polarimetric profile structure. However, it is found in other symbiotic systems that the spectropolarimetric profiles of the two Raman lines are very similar for all cases where they are strong enough to be compared (see e.g. Harries & Howarth 1996).

The spectropolarimetric structure of the Raman lines in HM Sge is very typical for symbiotic systems. A double-peaked intensity spectrum, a high percentage polarization in the blue part of the line, a decrease in polarization and an angle rotation or flip towards longer wavelength, and an enhanced polarization in the red line wing are all properties, which are also observed in systems like RR Tel and V1016 Cyg and many others (e.g. Schmid & Schild 1994; Harries & Howarth 1996; Schmid 1998). Even very subtle properties like a weaker blue peak in the λ7082 line compared to the λ6825 line (Fig. 1) is shared by many other symbiotic systems. This similarity is particularly interesting because the Raman lines in HM Sge just appeared for the first time and are still much weaker than in similar systems (RR Tel, V1016 Cyg).

5.3. The orientation of the binary axis

The polarization angle in the Raman scattered lines reflects the orientation of the scattering geometry as projected on the sky. Raman scattering by neutral hydrogen is a dipole type scattering process, which produces light polarization perpendicular to the incoming beam. In symbiotic systems strong O VI emission is expected to originate from near the hot component while the scattering by neutral hydrogen occurs in the neutral atmosphere and wind of the cool giant. In such a situation the orientation of the binary axis (the line connecting the two stars) is perpendicular to the polarization angle θ in the Raman lines. From this we infer that in June 1998 the orientation of the binary axis of HM Sge was about $\theta + 90° = 123°$.

As can be seen in Fig. 4 the polarization position angle through the Raman line is not constant. However the dominating polarization component is in the blue part of the line ($\lambda < 6830$ Å), where the position angle is almost constant. Therefore the integrated line polarization has practically the same position angle as the blue part of the line.

The proposed scattering models for the Raman lines in symbiotic systems (Schmid & Schild 1994; Schmid 1996; Harries & Howarth 1996,1997; Lee & Lee 1997a,b) suggest that the polarization in the blue line wing represents best the orientation of the binary axis. According to these models the photons in the blue wing are produced predominantly in the neutral region between the two stars. There the scattering H^0-atoms in the giant's wind are expected to move towards the O VI source. This produces due to the Doppler effect, blue shifted Raman photons. Contrary to this the photons in the red line wing originate mainly in the outer wind region, which recedes from the O VI source. Thus the inner region producing the blue line photons is relatively small and the corresponding scattering geometry is probably well aligned with the binary axis. This is supported by observation of other symbiotic systems. For example the polarization minima in the eclipsing system HBV 475 (V1329 Cyg) coincide well with conjunction (Schild & Schmid 1997). On the other hand it is known that the rotation of the polarization angle with the binary orbit scatters in some systems by about $5° - 10°$ from a strict orbital solution. Such deviations may be related to strong hydrodynamical interactions of the stellar winds. The position angle scatter was measured in short period ($P \approx 1 - 3$ yr) symbiotic systems and it can be expected that similar effects are smaller for HM Sge with its much larger binary separation and slower orbital motion.

6. Discussion

6.1. Dust evolution

We detected strong and unexpected spectral changes in the symbiotic system HM Sge:

- The continuum of the cool Mira has reappeared in the $7500-9000$ Å range.
- The Raman scattered O VI lines at $\lambda\lambda$6825,7082 have emerged
- The Lyβ–O I-fluorescence line at λ8446 has strengthened.

These spectral changes indicate that the dust content in HM Sge has decreased and hence, that the dust obscuration phase, which started in 1985, has ceased. Similar dust obscuration episodes are often observed in symbiotic Miras (e.g. Whitelock 1987). They typically last for several pulsation periods. Similar obscuration phases do not occur in single Miras. This indicates that the phenomenon is related to the binary nature of symbiotic systems. It has been suggested that these events could be due to an orbital eclipse mechanism. However, the high incidence of such obscurations in symbiotic Miras is not easily compatible with the expected orbital periods and a random orientation of the orbital planes. It is more likely that the already high dust formation rate in a Mira wind is further increased in matter concentrations generated by the presence of a companion object. Such condensations can be produced by the mere presence of an obstacle in the wind but will be enhanced if the companion object has a wind of its own or suffers an episodic outburst with an associated nova-like outflow.

6.2. Spectropolarimetry and binary orientation

Our spectropolarimetry shows that in HM Sge the red giant emission is intrinsically polarized. This is most likely due to light scattering in an aspherical photosphere. Earlier polarimetric data indicates that the intrinsic polarization of the red giant was already present prior to the dust obscuration event (Schulte-Ladbeck 1985). During dust obscuration the cool giant was too weak to produce an easily measurable polarization signal in the $\lambda < 1\mu$ region but intrinsic polarization was still present in the JHK-bands (Johnson & Jones 1991).

The polarization in the Raman scattered emission feature at λ6825 reflects the scattering geometry and hence the matter distribution in the inner binary system. In HM Sge the polarization angle is constant in the blue part of the Raman line and flips by 90 ° in the red part. Profiles of this type are easily understood in terms of an axisymmetric scattering geometry (Schmid & Schild 1994). Any asymmetries would immediately lead to a different profile like e.g. the one observed in V1016 Cyg where a slowly rotating polarization angle indicates a warped scattering geometry (Schild & Schmid 1996). We therefore conclude that, at least as far as the O VI–H I scattering geometry is concerned, the matter distribution in the inner HM Sge system is largely symmetrical with respect to the binary axis. In this case the observed polarization angle is perpendicular to the binary axis and we measure, that in June 1998, the connecting line between the two stars was at a position angle of ~ 123 °.

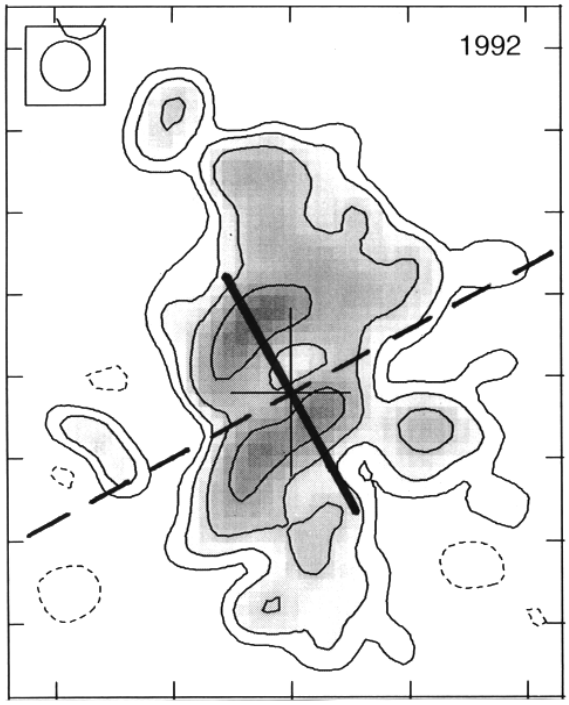

Fig. 5. Position angle of the Raman line polarization (thick line) and deduced orientation of the binary axis (dashed line) with respect to the 5 GHz Merlin radio map of HM Sge from 1992 (taken from Richards et al. 1999). One tick mark on the vertical axis corresponds to 0.1″. North is up and east to the left.

It is very interesting to compare this binary orientation with the sub-arcsec nebular structure from high resolution maps of HM Sge. Hack & Paresce (1993) detect on UV images (filter F190M) taken with HST in 1992 a nebulosity elongated in the southeast-northwest direction. Radio images taken almost simultaneously with Merlin associate this structure with two elongated and parallel emission ridges with a position angle of $\sim 120°$ (Eyres et al. 1995). The angular coincidence of these emission features with the polarimetrically deduced binary axis is noteworthy. In Fig. 5 the orientation of the binary axis with respect to these radio features is illustrated. As the binary period of HM Sge is certainly very long the time difference between the 1992 map and our polarimetry inserts a negligible error.

In more recent radio images these two ridges become less conspicuous and a central emission source emerges (Richards et al. 1999). The overall orientation of the inner 0.2″ nebulosity is now elongated perpendicular to the inferred binary axis.

HM Sge exhibits also a much larger but weak nebulosity extending to about 15″ from the center. Its morphology is very complex including outside the bright core a curved, collimated and knotty structure and a faint, diffuse component (Corradi et al. 1999). Based on high resolution spectroscopy the collimated structure was interpreted as bipolar outflows with radial velocities of ± 46 km/s at about 0.7″ from the center (Solf 1984). Most interesting is the orientation of this collimated structure,

which is $-60°$ or equivalent to $120°$, again aligned with the deduced binary axis. On larger scales this bipolar structure connects to two collimated structures several arcsec away which are decelerated and bend from northwest towards north and from southeast towards south respectively (Corradi et al. 1999).

In the course of time the orientation of the binary axis will change with the binary motion. The orbital period of HM Sge is unknown but certainly rather long. Richards et al. (1999) find with more recent radio images that some of the inner features at about $0.1''$ from the source center are rotating rather than expanding. If this rotation is, as suggested by the authors, linked to the orbital motion we should see a corresponding rotation in the binary axis as deduced from the Raman line polarization. However there are also other changes in the radio images connected with relative brightness changes between the two ridges and the central emission source. Thus, the structure of the nebulosity seen is rather complex and still evolving.

Summarizing, we find that the orientation of the binary axis in HM Sge deduced from the polarization in the Raman lines coincides with special orientations of the surrounding nebulosity. On the arcsec scale the binary axis is aligned with two collimated structures seen in the [O II] and [N II] filter images of Corradi et al. (1999). At smaller scales the binary axis is also aligned with two emission ridges seen in the 1992 radio map (see Fig. 5). Further we find that the binary axis is perpendicular to the elongation of the inner sub-arcsec nebulosity. These coincidences between the binary axis and distinct nebular features indicate that the orientation of the binary system is of prime importance for the understanding of the geometric structure of the nebulosity.

Various models have been proposed for the geometric structure of the nebulosity around HM Sge (e.g. Kwok et al. 1984; Solf 1984; Eyres et al. 1995; Richards et al. 1999). We therefore refrain from proposing a new model. However we like to emphasize that the orientation of the binary axis as deduced from the Raman line polarization adds now a new important piece of information. In particular, our result is in contradiction to the orientation of the binary axis proposed in the model of Richards et al. (1999). We may expect that future polarization measurements of the Raman lines reveals the orbital rotation of the binary system. This information would clarify whether the different nebular features mapped with radio and optical observations are equatorial or polar structures with respect to the orbital plane.

Thus further observations, especially the combination of high resolution imaging techniques together with Raman spectropolarimetry can potentially reveal much more detailed information on the hydrodynamical evolution of the nebulosity. As HM Sge is up to now the best observed example for the evolution of an ionized nebula following a symbiotic nova outburst, it may provide a key for a better understanding of the formation of bipolar nebulae.

Acknowledgements. We are indebted to our La Palma support astronomer Chris Packman, who provided valuable help during the observations. We thank Anita Richards for providing a Merlin radio map of HM Sge. HMS acknowledges financial support by the Deutsche Forschungsgemeinschaft (KR 1053/6-1).

References

Andrillat Y., 1982, In: Friedjung M., Viotti R. (eds.) The Nature of Symbiotic Stars. IAU Coll. 70, Reidel, p. 47
Bowen I.S., 1947, PASP 59, 196
Boyle R.P., Aspin C., Coyne G.V., McLean I.S., 1986, A&A 164, 310
Ciatti F., Mammano A., Vittone A., 1977, A&A 61, 459
Corradi R.L.M., Schwarz H.E., 1995, A&A 293, 871
Corradi R.L.M., Schwarz H.E., 1997, In: Mikolajewska J. (ed.) Physical Processes in symbiotic binaries and related systems. Proceedings of the conference held at Koninki, Poland, p. 147
Corradi R.L.M., Ferrer O.E., Schwarz H.E., Brandi E., Garcia L., 1999, A&A 348, 978
Coyne G.V., Magalhaes A.M., 1979, AJ 84, 1200
Dokuchaeva O.D., 1976, IBVS 1189
Efimov Y.S., 1979, SvA Lett. 5, 352
Eyres S.P.S., Kenny H.T., Cohen R.J., et al., 1995, MNRAS 274, 317
Grandi S.A., 1980, ApJ 238, 10
Hack W.J., Paresce F., 1993, PASP 105, 1273
Harries T.J., Howarth I.D., 1996, A&AS 119, 61
Harries T.J., Howarth I.D., 1997, A&AS 121, 15
Hsu J.C., Breger M., 1982, ApJ 262, 732
Johnson J.J., Jones T.J., 1991, AJ 101, 1735
Kamath U.S., Ashok N.M., 1999, A&AS 135, 199
Kastner S.O., Bhatia A.K., 1995, ApJ 439, 346
Kwok S., Bignell R.C., Purton C.R., 1984, ApJ 279, 188
Landstreet J.D., Angel J.R.P., 1977, ApJ 211, 825
Lee H.W., Lee K.W., 1997a, MNRAS 287, 211
Lee K.W., Lee H.W., 1997b, MNRAS 292, 573
Munari U., Whitelock P.A., 1989, MNRAS 237, 45P
Mürset U., Nussbaumer H., 1994, A&A 282, 586
Mürset U., Schmid H.M., 1999, A&AS 137, 473
Nussbaumer H., Vogel M., 1990, A&A 236, 117
Richards A.M.S., Bode M.F., Eyres S.P.S., et al., 1999, MNRAS 305, 380
Rudy R.J., Meier S.R., Rossano G.S., et al., 1999, ApJS 121, 533
Schild H., Schmid H.M., 1996, A&A 310, 211
Schild H., Schmid H.M., 1997, A&A 324, 606
Schild H., Boyle S.J., Schmid H.M., 1992, MNRAS 258, 95
Schmid H.M., 1989, A&A 211, L31
Schmid H.M., 1996, MNRAS 282, 511
Schmid H.M., 1998, Rev. in Mod. Astronomy 11, 297
Schmid H.M., Schild H., 1990, MNRAS 246, 84
Schmid H.M., Schild H., 1994, A&A 281, 145
Schmid H.M., Schild H., 1997, A&A 321, 791
Schulte-Ladbeck R., 1985, A&A 142, 333
Schulte-Ladbeck R., 1988, A&A 189, 97
Serkowski K., Mathewson D.L., Ford V.L., 1975, ApJ 196, 261
Solf J., 1984, A&A 139, 296
Stauffer J.R., 1984, ApJ 280, 695
Stover R.J., Sivertsen S., 1977, ApJ 214, L33
Tinbergen J., Rutten R., 1997, Measuring polarization with ISIS. Users' manual, The Isaac Newton Group of Telescopes, http://www.ing.iac.es/
Trammell S.R., Dinerstein H.L., Goodrich R.W., 1994, AJ 108, 984
Turnshek D.A., Bohlin R.C., Williamson R.L., et al., 1990, AJ 99, 1243
Whitelock P.A., 1987, PASP 99, 573
Yudin B., Munari U., Taranova O., Dalmeri I., 1994, A&AS 105, 169